Journal of Power Sources 196 (2011) 9544–9551

Contents lists available at ScienceDirect

Journal of Power Sources

journal homepage: www.elsevier.com/locate/jpowsour

Ex situ and modeling study of two-phase flow in a single channel of polymer electrolyte membrane fuel cells

Xavier Cordobes Adroher, Yun Wang*

Renewable Energy Resources Lab (RERL) and National Fuel Cell Research Center, Department of Mechanical and Aerospace Engineering, The University of California, Irvine, CA 92697-3975, USA

ARTICLE INFO

Article history:
Received 21 June 2011
Received in revised form 23 July 2011
Accepted 24 July 2011
Available online 4 August 2011

Keywords:
PEM fuel cells
Two-phase flow
Ex situ experiment
Two-fluid model
Flow patterns
Two-phase pressure amplifier

ABSTRACT

In this study, we investigate the air–water two-phase flow in a single flow channel of polymer electrolyte membrane (PEM) fuel cells. In the ex situ study, both straight and serpentine channels with various gas diffusion layer (GDL) surfaces are studied. Focus is placed on the two-phase flow patterns, which are optically characterized using a microscope with a high-resolution camera, and the two-phase pressure amplifiers. We find that the GDL surface properties slightly affect the flow pattern and two-phase pressure amplifier in the flow field configuration. Flow pattern transition occurs at the superficial gas velocity of around 1 m s^{-1}, and the pressure amplifier can reach as high as 10. A two-fluid model is also presented together with one dimensional (1-D) analytical solution, and acceptable agreement is achieved between the model prediction and experimental data at high gas flow rates.

1. Introduction

Polymer electrolyte membrane (PEM) fuel cells, which convert the chemical energy stored in hydrogen fuel directly and efficiently to electrical energy with water as the only by-product, have the potential to reduce our energy use, pollutant emissions, and dependence on fossil fuels [1,2]. Gas flow channels are an important fuel cell component for reactant supply and water removal. The surface of gas diffusion layers (GDL) constitutes one wall of a gas flow channel, playing an important role in the water management of fuel cells [3,4].

Air–water two-phase flow has been the focus of many studies. An important issue is to classify different types of flows. Flow regimes can be displayed in a flow regime map [5–7] with superficial gas and liquid velocities as coordinates. Typical patterns include bubbly, plug, slug, slug-annular, dispersed and annular flows. The frictional pressure drop ΔP_f is another important parameter, which can be characterized using the two-phase flow multiplier defined as the ratio of the two-phase pressure drop to the single-phase one [8–10]. In PEM fuel cells, the presence of liquid water increases ΔP_f in gas channels [11–15]. Wang et al. explained that the increased ΔP_f due to water accumulation is one important cause for flow mal-distribution, and that the two-phase flow multiplier may be a reliable indicator of water buildup in channels [14,15].

Liquid water in channels can be visualized using optical methods [16–22]. Tuber et al. were among the first groups to analyze water accumulation in a gas channel using a transparent fuel cell [16]. Lu et al. designed an experimental setup with 0.7 mm inner diameter channels and showed three flow regimes [19]. Neutron radiography investigations reported that higher water retention may be found at the U-bends of the serpentine channels [23], and that the use of hydrophobic coating on the gas channels leads to larger water retention. Modeling has been conducted by many studies in the area of two-phase channel flows. Most used the volume of fluid (VOF) method, which tracks the liquid–air interface. However, the VOF approaches are usually numerically expensive, therefore it is difficult to extend it to couple with the electrochemical kinetics and other transport mechanisms in a fuel cell model. In this regard, an engineering sub-model that is able to describe the important features of the two-phase channel flows and can be efficiently incorporated into a fuel cell model is highly desirable.

In this work, ex situ experiment is conducted to examine the characteristics of the two-phase flows in a single flow channel of a fuel cell. A two-fluid model is presented and its analytical solution to the experimental case is derived. The model prediction compares with the experimental data in terms of two-phase pressure amplifier. In addition, though many in situ studies were conducted previously to reveal the flows inside fuel cell channels, it is difficult to characterize the two-phase flows for modeling purpose

* Corresponding author. Tel.: +1 949 824 6004; fax: +1 949 824 8585.
E-mail address: yunw@uci.edu (Y. Wang).

0378-7753/$ – see front matter © 2011 Elsevier B.V. All rights reserved.
doi:10.1016/j.jpowsour.2011.07.076

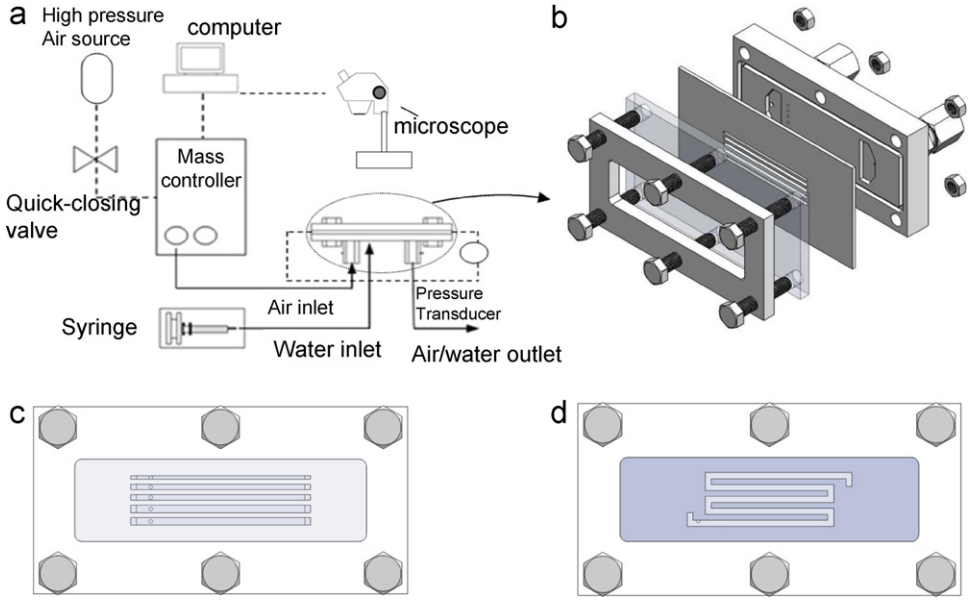

Fig. 1. (a) Schematic of the experimental setup; (b) detailed view of the experimental device; (c) the straight channel flow field (only the 3rd channel will be tested); and (d) the serpentine flow field.

because the in situ flow rate varies along the channel due to local water production by fuel cells. Ex situ experimental data under well controlled flow conditions are particularly important for the initial stage of model development.

2. Two-phase flows in the flow fields of PEM fuel cells

In fuel cells, water is produced in the cathode. Liquid emerges when the partial vapor pressure reaches the saturated one, and eventually enters the channel via the GDL, resulting in air–water two-phase channel flow. The water in channels can accumulate to a degree that greatly affects reactant supply. The water generated rate can be expressed using the Faraday law:

$$S_w = \frac{I}{2F} \tag{1}$$

The net water transport coefficient α is frequently adopted to calculate the net water gain in the cathode:

$$S_w^c = (1 + 2\alpha)\frac{I}{2F} \tag{2}$$

Assuming all the water addition is in liquid form when entering channels, integrating the above flux over a fuel cell yields the liquid flow rate in the cathode channel. The inlet gas flow rate is determined by the stoichiometric ratio ξ_c:

$$\vec{u}_{in,c} \cdot \vec{n}\big|_{\text{inlet}} = -\frac{\xi_c I A_m}{4FC_{O_2}A_c} \tag{3}$$

where A_c and A_m are the flow cross-sectional areas of the cathode gas channels and the membrane area, respectively. For a typical condition of 2 atm, 80 °C, 1.5 stoichiometry, and 1 A cm^{-2}, the gas velocity is in the magnitude of 1 m s^{-1}.

In gas channels, flow regimes can be displayed using the superficial gas (U_G) and liquid (U_L) velocities as coordinates:

$$U_G = \frac{\dot{m}x_G}{\rho_G} \quad \text{and} \quad U_L = \frac{\dot{m}x_L}{\rho_L} \tag{4}$$

where x_G and x_L are the qualities of gas and liquid, respectively, and $\dot{m}$ the mass flux. The frictional pressure drop (ΔP_f) is an important parameter characterizing two-phase flows, and its correlation can be developed using the concept of the two-phase flow multiplier ϕ_G^2 [8,9]:

$$\phi_G^2 = \frac{-(\partial P/\partial z)_{fr2\phi}}{-(\partial P/\partial z)_{frG}} \tag{5}$$

Chisholm examined the Lockhart–Martinelli correlating procedure and gave the pressure multiplier for pipe two-phase flows [10]:

$$\phi_G^2 = 1 + CX + X^2 \tag{6}$$

where X is the Lockhart–Martinelli parameter. Mishima et al. indicated that the coefficient C can depend on the micro-channel diameter [24]:

$$C = 21(1 + e^{-0.319D_h}) \tag{7}$$

where the hydraulic diameter is defined as:

$$D_h = \frac{4 \times \text{cross sectional area}}{\text{channel perimeter}} \tag{8}$$

3. Experimental

In experiment, the air–water two-phase flow was generated in a horizontal channel with controlled flow rates, see Fig. 1. The cross section of flow channels is rectangular with a 1.6 mm width and 1 mm height. The distance between the air inlet and outlet is 50 mm for the straight channel. The header has a dimension of ~10 mm × 5 mm × 1 mm. Three types of GDL surfaces are considered: smooth aluminum, carbon cloth, and carbon paper. Both the carbon cloth and paper are treated hydrophobic with 30% PTFE content. The side walls of the channels are made of aluminum, while the top uses a hydrophilic polycarbonate plate to facilitate optical access. Fig. 2 displays the water droplet shapes over the aluminum (contact angle ~50°) and polycarbonate plates (contact angle ~70°), respectively. Fig. 1(b) shows a detailed view of the test section. The gaseous phase was fed by a mass flow controller. Water was introduced to the channel through a ~0.1 mm diameter circular hole located on the bottom of the channel (GDL side), close to the air inlet. Water flow rate was controlled by a Chemyx Inc. Fusion 400 micro pump. Absolute and relative pressure measurements were

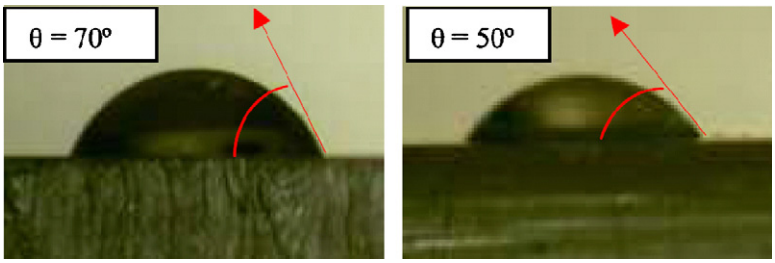

Fig. 2. The pictures of droplets over polycarbonate (left) and aluminum (right) surfaces.

taken by a pressure transducer. An overhead microscope and camera were used to record the images of the flow regimes. Fig. 1(a) shows the schematic of the overall experimental setup. The superficial gas velocity in the flow channel U_G varies from 0.44 m s^{-1} to 5.56 m s^{-1}, and the liquid one U_L from 1.1×10^{-4} to 5.5×10^{-3} m s^{-1} for most cases. It is worthy to mention that the considered region includes a flow channel and headers (also called manifolds) for the pressure drop measurement. Further in real PEFC operation, liquid water comes out of the GDL surface via multiple pores. We hope through this single-pore case, i.e. the single liquid injection port, we can verify the model and further extend it to our future study on more realistic condition.

4. A two-fluid model

Due to the mini/micro-scale nature of the channel dimension, the internal two-phase flow can be treated as flows in porous media [14,15]. The mass exchange occurs at the phase interface through water evaporation or condensation. The mass conservation of each phase can be written as follows [15]:

$$\text{Gas phase mass conservation}: \quad \nabla \cdot (\rho_g \vec{u}_g) = S_m^{fg} \tag{9}$$

$$\text{Liquid phase mass conservation}: \quad \nabla \cdot (\rho_l \vec{u}_l) = -S_m^{fg} \tag{10}$$

where $\vec{u}_g$ and $\vec{u}_l$ are the superficial velocities of gas and liquid, respectively. The gas density can be calculated through the constituent species:

$$\rho_g = \sum_k M_k C_k \tag{11}$$

Here, k represents species. In the cathode, there are nitrogen, water, and oxygen.

Flow in the porous media is driven by the pressure gradient and body forces, balanced with the shear stress at the solid surface. By adopting the Darcy's law and neglecting the gravitational force, the momentum equations can be written as:

$$\text{Gas phase momentum conservation}: \quad \rho_g \vec{u}_g = -\frac{k_{rg} K}{\nu_g} \nabla P_g \tag{12}$$

$$\text{Liquid phase momentum conservation}: \quad \rho_l \vec{u}_l = -\frac{k_{rl} K}{\nu_l} \nabla P_l \tag{13}$$

The relative permeabilities, k_{rg} and k_{rl}, are defined as the ratio of the intrinsic permeability of liquid/gas phase to the total permeability of a porous medium. Physically, it describes the extent to which one fluid is hindered by others in pore spaces and can be approximated as a function of liquid saturation. A set of functions have been frequently used in the fuel cell literature for the relative permeabilities:

$$k_{rl} = s_e^{n_k} \quad \text{and} \quad k_{rg} = (1 - s_e)^{n_k}$$

$$\text{where the effective saturation} \quad s_e = \frac{s_l - s_{ir}}{1 - s_{ir}} \tag{14}$$

Within the channel, water transport takes place in either gas or liquid phase. Note that the liquid phase is purely water. One can derive the water conservation as:

$$\nabla \cdot \left(\vec{u}_g C_g^{H_2O} + \vec{u}_l \frac{\rho_l}{M^{H_2O}} \right) = \nabla \cdot (\varepsilon s_g D_g^{H_2O} \nabla C_g^{H_2O}) \tag{15}$$

For analysis purpose, we consider one dimension (1-D) along the channel or x direction. We define a dimensionless $\bar{x}^*$, scaled by the length of the channel, as the location the liquid is injected. Before $\bar{x}^*$, the air flow is in the single-phase flow regime. After $\bar{x}^*$, liquid starts to form, resulting in two-phase transport. One can integrate both mass conservation equations from $\bar{x}^*$ to $\bar{x}$

$$\rho_g u_g = \rho_g(\bar{x}^*) u_g(\bar{x}^*) + \frac{L_x}{L_z} \int_{\bar{x}^*}^{\bar{x}} (S_m^{fg} + \beta S_m) d\hat{x} \tag{16}$$

$$\rho_l u_l = \frac{L_x}{L_z} \int_{\bar{x}^*}^{\bar{x}} (-S_m^{fg} + (1 - \beta) S_m) d\hat{x} \tag{17}$$

where S_m and β are the mass addition and the mass fraction of water addition in form of vapor from the channel wall, respectively. Note that in this case S_m is zero in the entire region except the location of $\bar{x}^*$. By neglecting diffusion, applying the same integration over the water conservation equation yields:

$$u_g C_g^{H_2O} + u_l \frac{\rho_l}{M_{H_2O}} = u_g(\bar{x}^*) C_{g,sat}^{H_2O} + \frac{L_x}{L_z} \int_{\bar{x}^*}^{\bar{x}} S^{H_2O} d\hat{x} \tag{18}$$

where S^{H_2O} is the water addition rate from the channel wall. Note that in this case S^{H_2O} is zero in the entire region except the location of $\bar{x}^*$.

Assuming the interfacial area between liquid and gas phases is large, the equilibrium between liquid and gas phases holds true, i.e. $C_g^{H_2O}$ equals to $C_{g,sat}^{H_2O}$. Assuming a constant gas density ρ_g, one can solve the phase superficial velocities

$$u_l = \frac{L_x M^{H_2O}}{L_z \rho_l (C_{g,sat}^{H_2O} M^{H_2O} - \rho_g)} \left(C_{g,sat}^{H_2O} \int_{\bar{x}^*}^{\bar{x}} S_m d\bar{x} - \rho_g \int_{\bar{x}^*}^{\bar{x}} S^{H_2O} d\hat{x} \right) \tag{19}$$

and

$$u_g = u_g(\bar{x}^*) - \frac{L_x}{L_z (C_{g,sat}^{H_2O} M^{H_2O} - \rho_g)} \left(\int_{\bar{x}^*}^{\bar{x}} S_m d\bar{x} - M^{H_2O} \int_{\bar{x}^*}^{\bar{x}} S^{H_2O} d\hat{x} \right) \tag{20}$$

Further, the Darcy's laws for both phases can be written in one dimension as

$$u_g = -\frac{k_{rg} K}{\mu_g} \frac{dP_g}{dx} \tag{21}$$

$$u_l = -\frac{k_{rl} K}{\mu_l} \frac{dP_l}{dx} = -\frac{k_{rl} K}{\mu_l} \left(\frac{dP_g}{dx} - \frac{dP_c}{dx} \right) \tag{22}$$

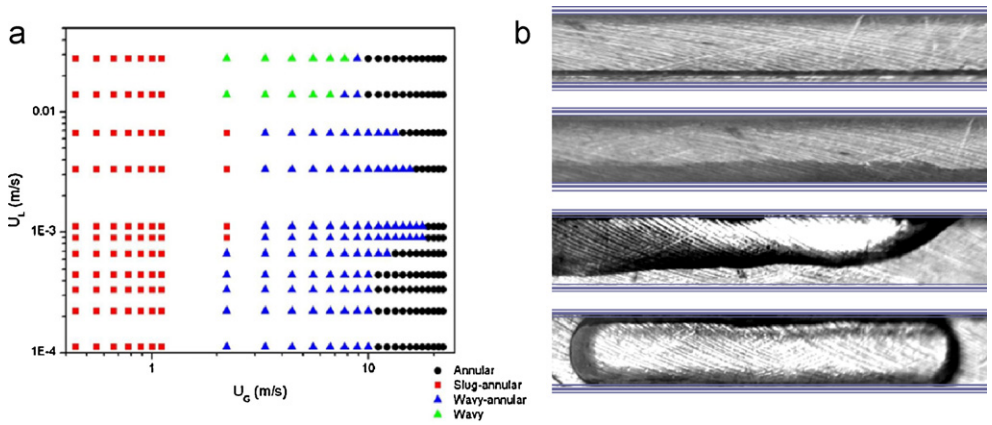

Fig. 3. Flow patterns of two-phase flow in the straight channel without GDLs (a). From the above to the bottom, the flow patterns are annular, wavy-annular, wavy, and slug-annular flows (b).

Combining these two equations to eliminate (dP_g/dx) and then substituting the Leverett J-function yields:

$$u_l = \frac{\mu_g}{\mu_l}\frac{k_{rl}}{k_{rg}}u_g + \frac{k_{rl}(K\varepsilon)^{1/2}\sigma\cos(\theta_c)}{\mu_l L_x}\frac{dJ}{ds}\frac{ds_l}{d\bar{x}} \tag{23}$$

The above equation can be solved numerically. To simplify the analytical solution, one can assume the liquid transport along the channel is primarily driven by the two-phase interaction through the shear stress, and the capillary action is small and negligible [15]. Therefore the above equation can be resolved explicitly:

$$s_l = \frac{(u_l\mu_l/\mu_g u_g)^{(1/n_k)} + s_{ir}}{1 + (u_l\mu_l/\mu_g u_g)^{(1/n_k)}} \tag{24}$$

Once the saturation profile is available, the relative permeabilities can be calculated, which are further substituted to the pressure equations

$$P_g = P_g(\bar{x}^*) - L_x\int_{\bar{x}^*}^{\bar{x}}\frac{\mu_g u_g}{k_{rg}K}d\hat{x} \tag{25}$$

$$P_l = P_g(\bar{x}^*) - L_x\int_{\bar{x}^*}^{\bar{x}}\frac{\mu_l u_l}{k_{rl}K}d\hat{x} \tag{26}$$

The total pressure drop of the gas-phase along the porous channel will be:

$$\Delta\bar{P}_g = \frac{\Delta P_g}{(\mu_g u_{g,in}L_x)/K} = \int_0^{\bar{x}^*}\frac{u_g}{u_{g,in}}d\hat{x} + \int_{\bar{x}^*}^{1}\frac{u_g}{u_{g,in}}\frac{1}{k_{rg}}d\hat{x} \tag{27}$$

Assuming a constant air superficial velocity, the pressure scale (i.e. the denominator in the middle term of the above equation) becomes the pressure drop for a single-phase flow. The above equation can further be rearranged as

$$\Delta\bar{P}_g = \bar{x}^* + \int_{\bar{x}^*}^{1}\frac{1}{k_{rg}}d\hat{x} \tag{28}$$

It is worth to note that the above dimensionless pressure is defined in the same way as the two-phase pressure amplifier ϕ_G^2 in Eq. (5). Detail regarding the two-fluid flow model and analysis can be found in Ref. [15] for fuel cells.

5. Results and discussion

Fig. 3(a) displays the two-phase flow regime map for the straight channel without GDLs, i.e. the GDL side is an Aluminum surface. Fig. 3(b) shows several typical flow patterns observed. It can be seen that with decreasing gas flow rate the two-phase flow experiences annulus, wavy annulus, wavy, and slug in the range of considered operating condition. The shear stress exerted by the gas stream is a major driven force for liquid flow. When there lacks of a sufficient gas flow, liquid accumulates, forming slug flow. When the gas flow becomes strong, the two-phase stream is stable annulus with liquid over the channel walls. Fig. 4 presents comparison with other observations [19,25], showing an acceptable agreement.

Fig. 5 displays the two-phase pressure amplifier profiles and comparison with the Lockhart–Martinelli correlation and model prediction. The pressure amplifier represents the effect of liquid presence on the pumping pressure required to drive the gas flow.

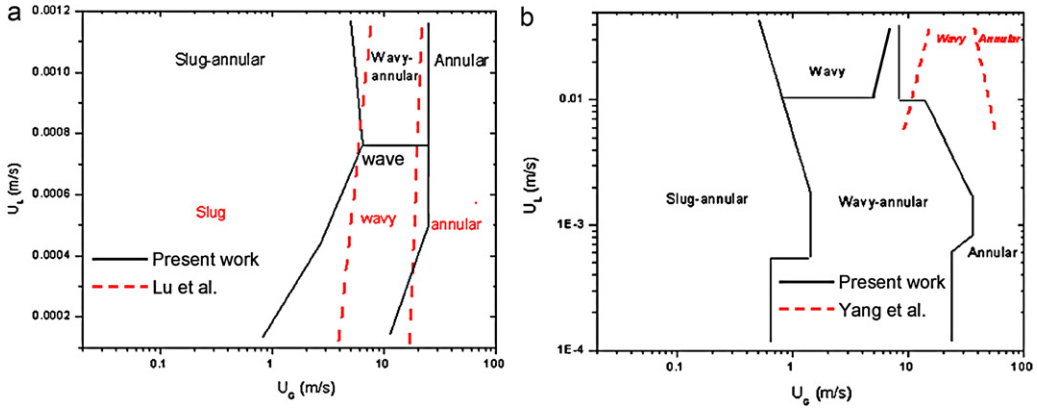

Fig. 4. Comparison with the results obtained by: (a) Lu et al. [19], using a 0.7 mm inner diameter circular tube; and (b) Yang et al. [25], using a 1 mm inner diameter circular tube.

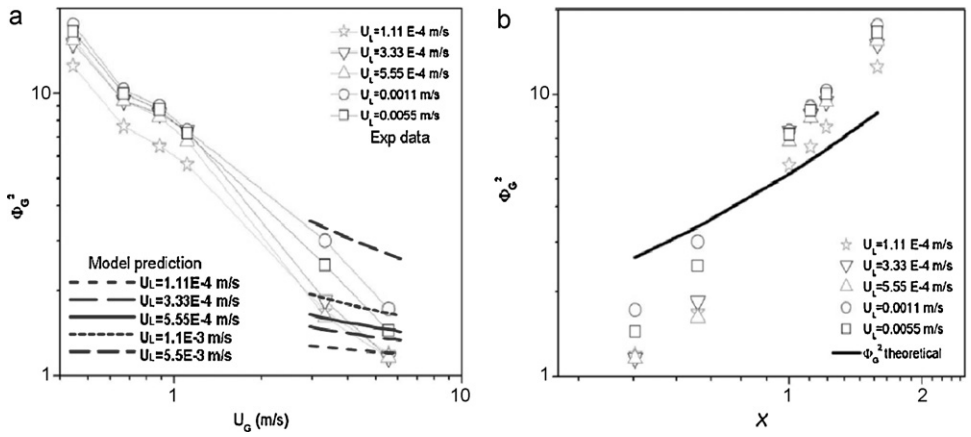

Fig. 5. ϕ_G^2 as a function of U_G and U_L from model prediction and experiment (a); and comparison between the experimental and Lockhart–Martinelli values of ϕ_G^2 (b).

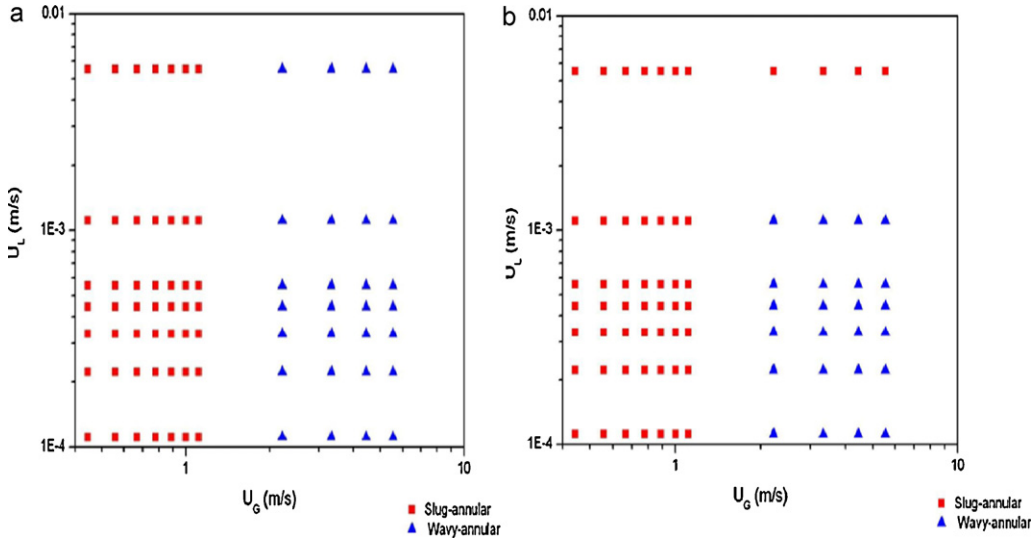

Fig. 6. Flow patterns in the straight channel with carbon cloth (a) and paper (b).

It can be seen from Fig. 5(a) that the value of the amplifier factor is close to 1 when the gas flow rate is high, and increases to around 10 at low gas flow rates. The liquid flow rate also affects the amplifier. The model predictions are also provided for higher gas flow rates. The model parameters are given in Table 1. It can be seen that the model predictions are in line with the experimental data for the considered region. For lower gas flow regions, the model parameters must be changed, for different liquid flow rates and GDL surfaces, in order to fit with the experimental data, which is likely due to the change in two-phase flow patterns. Further efforts are required to examine the various model parameters. We will present the results in our future work.

Fig. 5(b) compares the two-phase amplifier with the Lockhart–Martinelli correlation, indicating a reasonably good

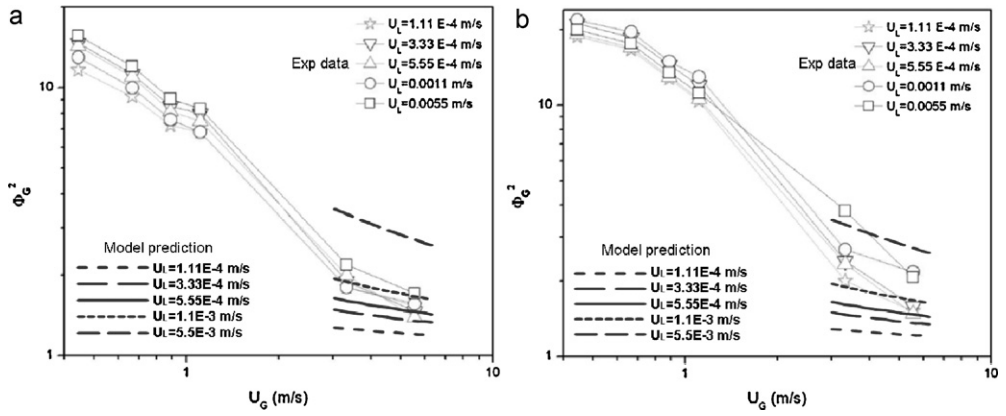

Fig. 7. Two-phase pressure amplifiers for straight channels with carbon cloth (a) and paper (b).

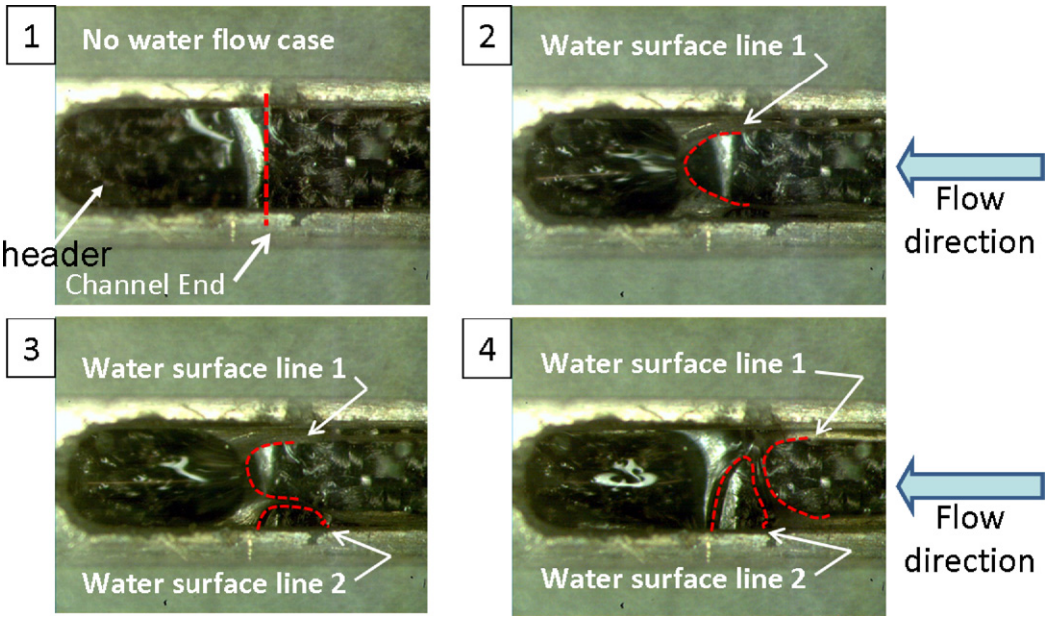

Fig. 8. Two-phase flow dynamics near the channel-header connection [30].

Table 1
Geometrical, physical and model parameters.

Quantity	Value
Gas channel depth/width	1.0/1.6 mm
Viscosity of liquid water, u_l	0.000894 kg m^{-1} s^{-1}
Viscosity of air, μ_g	1.86×10^{-6} kg m^{-1} s^{-1}
Residual liquid saturation, s_{ir}	0
Exponent in the relative permeability, n_k	2

agreement. We used the Mishima and Hibiki approach in order to calculate the coefficient C in the Chisholm equation [26]. It is worthy to mention that the gas pressure drop is closely related to the pumping power required to feed the reactants [27]. Another issue closely related to pressure drop is flow mal-distribution phenomena occurring among parallel channels. Assuming two channels in parallel follow the same trend of two-phase pressure amplifier, the two channels will have totally different air flow rates when subjecting to different flow regimes. Other investigations [28,29] also presented similar results of the two-phase pressure amplifier.

Figs. 6 and 7 display the two-phase flow regimes and pressure amplifiers for carbon cloth and paper. When using a hydrophobic surface in the GDL side, we found that visually distinguishing the wavy, annulus, and wavy annulus patterns becomes difficult due to the distinct wall properties between the GDL surface and channel side walls: the liquid free surface observed through the top transparent plate can be disturbed, i.e. wavy, even the flow still resides in the stable annulus regime. Therefore, for these two cases we only distinguish the slug-annulus and wavy-annulus patterns, i.e. the wavy-annulus pattern lumps the ones of wavy, wavy-annulus, and possible annulus. It can be seen that the two-phase flow regimes are similar between the carbon paper and cloth. The flow transition takes place at U_G of around 1 m s^{-1}. The model predictions are also plotted for comparison. It can be seen the agreement is acceptable.

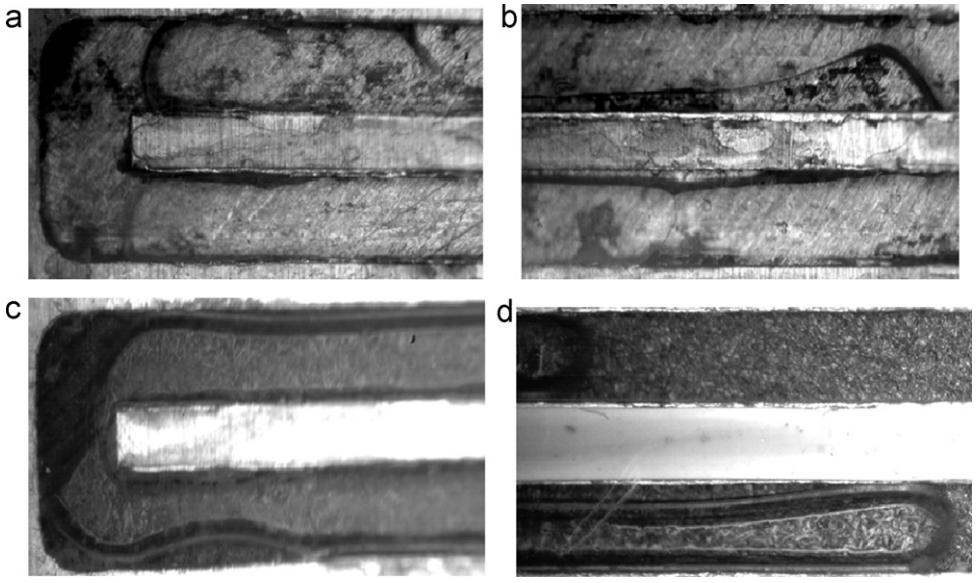

Fig. 9. Two-phase flow visualizations for the smooth aluminum surface: (a) and (b); for the carbon paper surface (c); and for the carbon cloth surface (d).

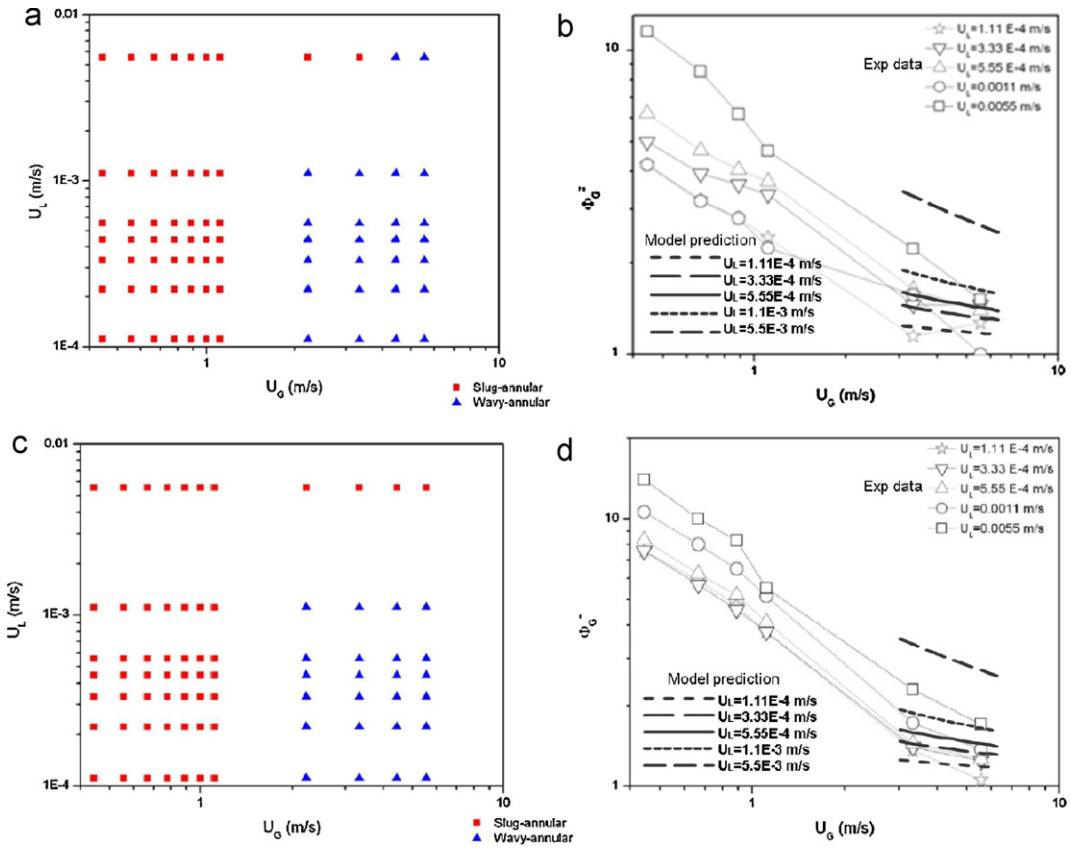

Fig. 10. Two-phase flow patterns and pressure amplifiers for a serpentine channel with the carbon cloth (a) and (b), and carbon paper (c) and (d), respectively.

Note that the model does not distinguish the GDL surface properties, therefore the model prediction results are the same as that in Fig. 5.

In comparison of the three cases, it can be seen that the difference is small, and the difference occurs primarily in the transition region. This is likely due to the difference in the surface properties, either wettability or roughness. In addition, we also find that at the connection between the flow channel and header, liquid accumulates in the header side and can block the channel at low gas flow rates, see Fig. 8, which shows the liquid surface dynamics near the channel outlet. Wang et al. indicated liquid will buildup near the interface between small and large channels due to heterogeneity [14]. This liquid build up may block the small channel due to the capillary action. Note that many designs of optical fuel cells have similar channel-header configuration. As to the two-phase pressure amplifier, the profiles exhibit similar trend among the three cases.

Another popular flow field in PEM fuel cells is the serpentine pattern, see Fig. 1(d). Liquid water may be trapped at the corners of the U-turns, see Fig. 9(a) and (c). The trapped water can be stripped off by gas flow, influencing the downstream flow, see Fig. 9(b). For comparison purpose, we put together the cases for the carbon paper and cloth, see Fig. 10. Again similar to the single-channel case the flow transition occurs around $U_G = 1.0\ \mathrm{m\,s^{-1}}$, indicating that the liquid accumulate near the corner has a small impact on the two-phase flow patterns, and the two-phase pressure amplifiers. This is possibly due to the fact that liquid accumulation at the U-turn is relatively slow given the small liquid water injection rate (usually the case in a fuel cell) and the stripped-off liquid, if forming slug, can be rapidly removed out of the short channel by gas flow in the timescale around 0.01–0.1 s, therefore imposing a small influence on the averaged two-phase pressure amplifiers. The model predictions are also plotted in Fig. 10(b) and (d). Again the agreement is acceptable.

6. Conclusions

This study conducted ex situ investigation and model analysis of air-water two-phase flows in a single-channel flow field of PEM fuel cells. The experiment examined two-phase flow patterns and pressures. We found altering the GDL surface properties may slightly change the flow patterns, and the liquid water can accumulate near the header-channel interface, affecting the channel flow. Flow pattern transition occurs around the gas velocity of $1\ \mathrm{m\,s^{-1}}$ for the considered channels, and the two-phase pressure amplifiers can reach about 10 at the gas velocity of $0.5\ \mathrm{m\,s^{-1}}$, and are reduced to 1 when the gas flow rate is sufficiently high. In the serpentine configuration, we found that the water trapped at the corner of the U-turn has a small impact on two-phase flow pattern and pressure amplifier for a single channel flow. A two-fluid model was presented for the experimental case with analytical solution derived. By comparison, we obtained an acceptable agreement with experimental data at high gas flow rates.

Acknowledgements

The Balsells program and the Mechanical and Aerospace Engineering Department of the University of California Irvine are gratefully acknowledged for financial support. The Renewable Energy Resources Laboratory's graduate students Liem Pham and Sung Chan Cho are acknowledged for their help in the preparation of this paper.

References

[1] C.Y. Wang, Fundamental model for fuel cell engineering, Chemical Reviews 104 (2004) 4727–4766.
[2] Y. Wang, K.S. Chen, J. Mishler, S.C. Cho, X.C. Adroher, A review of polymer electrolyte membrane fuel cells: technology, applications, and needs on fundamental research, Applied Energy 88 (2011) 981–1007.
[3] M.F. Mathias, J. Roth, J. Fleming, W. Lehnert, Diffusion media materials and characterization, in: Handbook of Fuel Cells – Fundamentals, Technology and Applications, John Wiley & Sons, 2003.
[4] Y. Wang, C.Y. Wang, K.S. Chen, Elucidating differences between carbon paper and carbon cloth in polymer electrolyte fuel cells, Electrochimica Acta 52 (2007) 3965–3975.
[5] J.M. Manhane, G.A. Gregory, K. Aziz, A flow pattern map for gas–liquid flow in horizontal pipeline, International Journal of Multiphase flow 1 (1974) 537–553.
[6] Y. Taitel, A.E. Dukler, A model for predicting flow regime transitions in horizontal and near horizontal gas–liquid flow, American Institute of Chemical Engineers 22 (1975) 47–55.
[7] D. Barnea, Y. Luninski, Y. Taitel, Flow pattern in horizontal and vertical two phase flow in small diameter pipes, Canadian Journal of Chemical Engineering 61 (1983) 617.
[8] R.W. Lockhart, R.C. Martinelli, Proposed correlation of data for isothermal two-phase, two-component flow in pipes, Chemical Engineering Progress 45 (1949) 39–48.
[9] R.C. Martinelli, B. Nelson, Prediction of pressure drop during forced-circulation boiling water, Transactions of the American Society of Mechanical Engineers 70 (1948) 695–702.
[10] D.A. Chisholm, A theoretical basis for the Lockhart–Martinelli correlation for two-phase flow, International Journal of Heat and Mass Transfer 10 (1967) 1767–1778.
[11] W. He, G. Lin, T.V. Nguyen, Diagnostic tool to detect electrode flooding in proton-exchange-membrane fuel cells, American Institute of Chemical Engineers 49 (2003) 3221–3228.
[12] H.P. Ma, H.M. Zhang, J. Hu, Y.H. Cai, B.L. Yi, Diagnostic tool to detect liquid water removal in the cathode channels of proton exchangemembrane fuel cells, Journal Power Sources 162 (2006) 469–473.
[13] X. Liu, H. Guo, F. Ye, C.F. Ma, Flow dynamic characteristics in flow field of proton exchange membrane fuel cells, International Journal Hydrogen Energy 33 (2008) 1040–1051.
[14] Y. Wang, S. Basu, C-Y. Wang, Modeling two-phase flow in PEM fuel cell channels, Journal Power Sources 179 (2008) 603–617.
[15] Y. Wang, Porous-media flow fields for polymer electrolyte fuel cells ii analysis of channel two-phase flow, Journal of the Electrochemical Society 156 (10) (2009) B1134–B1141.
[16] K. Tuber, D. Pocza, C. Hebling, Visualization of water buildup in the cathode of a transparent PEM fuel cell, Journal of Power Sources 124 (2004) 403–414.
[17] F.B. Weng, A. Su, C.Y. Hsu, C.Y. Lee, Study of water-flooding behavior in cathode channel of a transparent proton-exchange membrane fuel cell, Journal of Power Sources 157 (2006) 674–680.
[18] X. Liu, H. Guo, C. Ma, Water flooding and two-phase flow in cathode channels of proton exchange membrane fuel cells, Journal of Power Sources 156 (2006) 267–280.
[19] Z. Lu, S.G. Kandlikar, C. Rath, M. Grimm, W. Domigan, A.D. White, M. Hardbarger, J.P. Owejan, T.A. Trabold, Water management studies in PEM fuel cells. Part II: ex situ investigation of flow maldistribution, pressure drop and two-phase flow pattern in gas channels, International Journal of Hydrogen Energy 34 (2009) 3445–3456.
[20] X.G. Yang, F.Y. Zhang, A. Lubawy, C.Y. Wang, Electrochemical and Solid-State Letters 7 (2004) A408–A411.
[21] F.Y. Zhang, X.G. Yang, C.Y. Wang, Journal of the Electrochemical Society 153 (2006) A225–A232.
[22] K.S. Chen, M.A. Hickner, D.R. Noble, Simplified models for predicting the onset of liquid water droplet instability at the gas diffusion layer/gas flow channel interface, International Journal of Energy Research 29 (12) (2005) 1113–1132.
[23] T.A. Trabold, J.P. Owejan, D.L. Jacobson, M. Arif, P.R. Huffman, In situ investigation of water transport in an operating PEM fuel cell using neutron radiography: part I – experimental method and serpentine flow field results, International Journal of Heat and Mass Transfer 49 (2006) 4712–4720.
[24] K. Mishima, T. Hibiki, Some characteristics of air–water two-phase flow in small diameter vertical tubes, International Journal of Multiphase Flow 22 (1996) 703–712.
[25] C.Y. Yang, C.C. Shieh, Flow pattern of air–water and two-phase R-134a in small circular tubes, International Journal of Multiphase Flow 27 (2001) 1163–1177.
[26] K. Mishima, T. Hibiki, H. Nishihara, Some characteristics of gas–liquid flow in narrow rectangular ducts, International Journal of Multiphase Flow 19 (1993) 115–124.
[27] Y. Wang, Porous-media flow fields for polymer electrolyte fuel cells I. Low humidity operation, Journal of the Electrochemical Society 156 (10) (2009) B1124–B1133.
[28] Y. Chen, Y.M. Chen, B.C. Yang, C.C. Wang, Two-phase flow pattern and frictional performance across small rectangular channels, Applied Thermal Engineering 29 (2009) 1309–1318.
[29] S. Saisorn, S. Wongwises, Flow pattern, void fraction and pressure drop of two-phase air–water flow in a horizontal circular micro-channel, Experimental Thermal and Fluid Science 32 (2008) 748–760.
[30] S.C. Cho, Y. Wang, Private Communication.